Geophys. J. Int. (2008) **173,** 990–999 doi: 10.1111/j.1365-246X.2008.03781.x

Quantitative accuracy analysis of the discontinuous Galerkin method for seismic wave propagation

Martin Käser, Verena Hermann and Josep de la Puente

Department of Earth and Environmental Sciences, Geophysics Section, Ludwig-Maximilians-Universität, München, Germany.
E-mail: martin.kaeser@geophysik.uni-muenchen.de

Accepted 2008 March 5. Received 2008 February 27; in original form 2007 December 20

SUMMARY

We present a quantitative accuracy analysis of the Discontinuous Galerkin Finite-Element method for the simulation of seismic wave propagation on tetrahedral meshes. Several parameters are responsible for the accuracy of results, such as the chosen approximation order, the spatial discretization, that is, number of elements per wavelength, and the propagation distance of the waves due to numerical dispersion and dissipation. As error norm we choose the time–frequency representation of the envelope and phase misfit of seismograms to assess the accuracy of the resulting seismograms since this provides the time evolution of the spectral content and allows for the clear separation of amplitude and phase errors obtained by the numerical method. Our results can be directly used to set up the necessary modelling parameters for practical applications, such as the minimum approximation order for a given mesh spacing to reach a desired accuracy. Finally, we apply our results to the well-acknowledged LOH.1 and LOH.3 problems of the SPICE Code Validation project, including heterogeneous material and the free surface boundary condition, and compare our solutions with those of other methods. In general, we want to stress the increasing importance of certain standard procedures to facilitate future code validations and comparisons of results in the community of numerical seismology.

Key words: Time series analysis, Numerical solutions; Wavelet transform; Numerical approximations and analysis; Computational seismology; Wave propagation.

1 INTRODUCTION

Computational seismology has become an increasingly important discipline and might become more relevant with increasing computational resources as more realistic scenarios can be modelled. Within the last few decades, a number of different numerical methods has been developed. Starting from early staggered finite-difference (FD) schemes (Madariaga 1976; Virieux 1984, 1986), their improved and extended versions to viscoelastic material (Moczo *et al.* 2002) and the partly-staggered grid FD schemes (Saenger *et al.* 2000; Saenger & Bohlen 2004), the optimally-accurate FD schemes (Geller & Takeuchi 1995, 1998; Kristek & Moczo 2006) have become increasingly important. A recent review of the developments in FD modelling is given by Moczo *et al.* (2007a,b). Furthermore, the Fourier pseudospectral (PS) methods (Fornberg 1975; Carcione 1994; Fornberg 1996), finite-element (FE) approaches (Marfurt 1984; Bielak *et al.* 2003; Yoshimura *et al.* 2003; Koketsu *et al.* 2004; Moczo *et al.* 2007a), boundary integral equations (BIEM) and boundary element methods (BEM) (Bouchon & Sánchez-Sesma 2007) and spectral element methods (SEM) (Seriani & Priolo 1994; Komatitsch & Vilotte 1998; Chaljub *et al.* 2003, 2007; Komatitsch *et al.* 2004) have been developed. Rather recently, the Discontinuous Galerkin (DG) Finite-Element method has been introduced into numerical seismology (Käser & Dumbser 2006; Dumbser & Käser 2006) and extended to viscoelastic (Käser *et al.* 2007a) and anisotropic (de la Puente *et al.* 2007) media. Important technical improvements concerning adaptive approximation orders and local time stepping have been presented by Dumbser *et al.* (2007). As each method has its advantages and disadvantages that often depend on the particular application, it is difficult, if not impossible, to decide which method is best with respect to its performance. However, it is clear that today the interpretation of synthetic seismograms typically requires a high level of confidence and therefore numerical accuracy, where the numerical errors or artefacts do not affect true features in the seismogram due to the Earth's structure or the source properties. Therefore, the study of the accuracy of a numerical scheme is essential to evaluate its performance as well as its limits. As there is a relatively large number of different methods, it becomes more and more difficult for developers to compare their own approach with all other methods. To this end, Seismic wave Propagation and Imaging in Complex media: a European network (SPICE) has established a digital library (Gallovič *et al.* 2007), available at www.spice-rtn.org, to collect seismic wave propagation codes and analytical solutions as well as to facilitate comparisons between different methods based on common error norms.

In this work, we contribute to these comparisons and study the accuracy of the DG method combined with a time integration scheme using arbitrary high-order derivatives (ADER) as introduced recently for the simulation of seismic waves (Käser & Dumbser 2006). This scheme achieves high approximation orders in space and time on unstructured tetrahedral meshes as shown by Dumbser & Käser (2006) and is based on the finite-element approach. Here, we investigate the accuracy of the ADER-DG scheme in a way to facilitate the decisions that a modeler has to make when solving a practical problem: the desired accuracy of the synthetic seismograms; the spatial sampling of the computational domain (i.e. the mesh spacing); the maximum propagation distance of the waves and the required approximation order of the method. Note that here and in the following we use the term 'mesh spacing' in the sense relative to the background velocity structure. Therefore, the mesh spacing should always be understood as number of elements per wavelength. Furthermore, it is crucial to choose an error norm that describes the accuracy of a synthetic seismogram quantitatively and separates amplitude and phase misfits as shown by Kristeková *et al.* (2006). For this purpose, we simulate the propagation of a Ricker pulse in a 3-D domain with the ADER-DG method for different approximation orders, mesh spacings and propagation distances and carefully analyse the corresponding numerical errors. We then apply the ADER-DG method to problems given online through the SPICE Code Validation website (www.nuquake.eu/SPICECVal). Note that the original ideas of such a benchmarking exercise have been suggested by the SCEC Code Validation project (Day *et al.* 2003), however, the SPICE project extended and considerably improved these ideas by (a) covering systematically important categories of different problem configurations; (b) applying newest quantitative misfit criteria to compare the obtained solutions and (c) establishing and providing a long-term interactive database for uploading and comparing numerical solutions with analytical or reference solutions. Therefore, we use the SPICE Code Validation website to confirm the validity of our error analysis and to compare our simulation results with those obtained by other methods. The results of these other methods (so far only FD and FE results are available) are shown in detail by Kristeková *et al.* (2006).

2 ACCURACY ANALYSIS

The evaluation of the accuracy of a numerical method is a crucial issue to describe its performance and assess its applicability to practical problems. As the accuracy depends on a number of modelling parameters as mentioned above, general statements, for example, '6 points per wavelength are needed to correctly propagate a wave when using order 8', are too general, and therefore problematic, but unfortunately encountered commonly for many methods. Therefore, the numerical errors have to be analysed, dependent on at least the approximation order, the spatial sampling and the propagation distance.

A sound error analysis for three types of the FD method was carried out by Kristek & Moczo (2006), however, only for the 1-D case and a maximum propagation distance of 20 dominant wavelengths. They also include the optimally accurate scheme of Geller & Takeuchi (1998) in their analysis. Similarly, Fornberg (1987) shows an accuracy analysis for the PS method, however, he only uses a phase error estimator as error norm. Furthermore, Seriani & Priolo (1994) study the accuracy of the SEM showing the relative evolution of the numerical error depending on approximation order, spatial sampling and propagation distance, without giving absolute error values. Only for their heterogeneous test case, they provide the maximum absolute error of the seismograms. A more recent work on the SEM is presented by Ampuero & Nissen-Meyer (2008), who study the dispersion error of the SEM analytically and replace the typically used low-order Newmark time integration scheme with higher-order symplectic schemes. They prescribe an expected (i.e. data-driven) error tolerance and then extract optimal simulation parameters for that accuracy, such as the approximation order in space and time, to minimize the computational cost. Moreover, they also define errors for phase and amplitude separately. To this end, they use cross-correlation to determine the phase error and the root mean square (rms) to determine the amplitude misfit after shifting the seismogram by the phase error. It should be mentioned that these are alternative error measures of numerical seismograms since they also separate phase and amplitude misfits. However, the frequency dependence of the misfit cannot be estimated this way, which might be the main drawback. We remark that in some cases it can be extremely useful to capture the frequency band where a numerical method loses or produces energy, even though the initial source signal might have a different frequency band.

Therefore, we claim that the error norms suggested by Kristeková *et al.* (2006) should be mainly used in the future as they are based on the time–frequency representation of the seismogram misfit.

2.1 Time–frequency representation of the misfit

In numerical seismology, a simple and often used error norm is the difference seismogram between the numerical solution and a reliable reference solution, which visually provides a good first comparison, but is only a very qualitative measure. Furthermore, a simple integral criterion is the rms misfit. However, both measures quantify the difference between seismograms without distinguishing properly between amplitude or phase errors. In particular, the rms usually considerably overestimates the misfit as it wrongly attributes amplitude errors due to phase shifts. Therefore, Seriani & Priolo (1994) propose a frequency error index, which is a complex function given by the ratio of the Fourier transform of the numerical solution and the analytic solution. This way, they determine the minimum wavelength for which a numerical method is sufficiently accurate. By considering the real and imaginary parts of their frequency error index separately, they can distinguish between errors due to amplitude variations or velocity dispersion, that is, phase errors, respectively.

Recently, Kristeková *et al.* (2006) introduced new misfit criteria for quantitative comparisons of seismograms, which are based on the time–frequency representation (TFR) using the continuous wavelet transform. With the TFR of the misfit, they can extract the time evolution of the spectral content. Therefore, they define a local time–frequency envelope difference

$$\Delta E(t, f) = |W(t, f)| - |W_{\mathrm{ref}}(t, f)| \tag{1}$$

and a time–frequency phase difference

$$\Delta P(t, f) = |W_{\mathrm{ref}}(t, f)| \, \frac{\arg[W(t, f)] - \arg[W_{\mathrm{ref}}(t, f)]}{\pi}, \tag{2}$$

where $W(t, f)$ and $W_{\mathrm{ref}}(t, f)$ are the complex functions of the continuous wavelet transforms of the numerical and the reference seismograms, respectively. For a detailed description of the continuous wavelet transform, the reader is referred to the book of Holschneider (1995) and the free software package TF-MISFITS for signal analysis is available at www.nuquake.eu/Computer_Codes. Kristeková *et al.* (2006) also obtain purely time- or frequency-dependent quantities of the misfits by the projection onto one of the two domains.

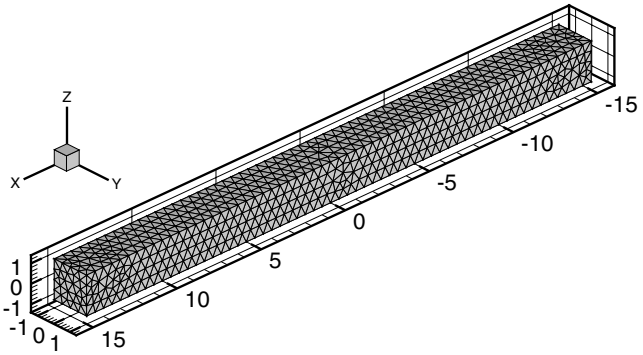

Figure 1. Computational domain discretized by Mesh 4 with periodic boundary conditions in the *x*-, *y*-, and *z*-directions applied to simulate the propagation of the Ricker-type plane wave in the *x*-direction for 120 wavelengths.

Here, we use their single-valued measures for the envelope misfit (EM) and phase misfit (PM) between two signals defined as

$$\mathrm{EM} = \sqrt{\frac{\sum_f \sum_t |\Delta E(t,\, f)|^2}{\sum_f \sum_t |W_{\mathrm{ref}}(t,\, f)|^2}} \quad \text{and}$$

$$\mathrm{PM} = \sqrt{\frac{\sum_f \sum_t |\Delta P(t,\, f)|^2}{\sum_f \sum_t |W_{\mathrm{ref}}(t,\, f)|^2}} \tag{3}$$

including the definitions (1) and (2). In the following, we apply these new misfit criteria to separate amplitude and phase errors to quantitatively analyse the performance of the ADER-DG scheme with respect to the approximation order, the mesh spacing, and the propagation distance of the waves.

2.2 Model setup

In the following, we describe in detail our computational setup for the numerical accuracy analysis in three dimensions so that comparisons can easily be produced by different methods. We use eleven different unstructured tetrahedral meshes discretizing a cuboid $\Omega = [-15, 15]\,\mathrm{m} \times [-1, 1]\,\mathrm{m} \times [-1, 1]\,\mathrm{m} \in \mathbb{R}^3$ elongated in the *x*-direction as shown in Fig. 1. The meshes are generated in a way that periodic boundary conditions in the *x*- *y*-, and *z*-direction can be applied. The mesh spacing Δh_k is represented by the average tetrahedral edge length of each of the meshes indicated by 'Mesh *k*', where $\Delta h_k = 2/k$, for $k \in [2, 3, 4, 5, 6, 8, 10, 12, 14, 16, 18]$. We use a plane wave with a Ricker-type amplitude distribution $A(x) = (1 - 2\tau^2)\exp(-\tau^2)$, with $\tau = 1.25\,\pi x$ and propagate it with wave velocity $c = 1\,\mathrm{m\,s^{-1}}$ in the positive *x*-direction. Therefore, an analytical seismogram is given by the same Ricker wavelet in time, as shown in Fig. 2(a), with a dominant frequency $f_d = 1.25$ Hz and hence a dominant wavelength $\lambda_d = 0.8$ m. The Fourier spectrum and the TFR of the used Ricker wavelet are shown in Figs 2(b) and (c), respectively. We remark, that we use a plane compressional wave in a homogeneous elastic medium. However, the wave could also represent a pure pressure wave in an acoustic medium or a pure shear wave in an elastic medium. Due to this generality, we will not refer to one particular type of planar wave here, but want to emphasize that always the slowest wave, that is, the shortest wavelength, has to be considered, when transforming these results to more complicated cases with different types of waves. The abovementioned parameters determine the number of elements per dominant wavelength $N_k = \lambda_d / \Delta h_k = 0.4\,k$ that each Mesh *k* provides for the wave propagation simulation. We solve the test problem with ADER-DG schemes of order 2 to order 7, indicated by ADER-DG $\mathcal{O}2$ to ADER-DG $\mathcal{O}7$, respectively.

The synthetic seismograms are recorded at 30 receivers equidistantly distributed along the *x*-axis at $\vec{x}_r = (r - 15.5,\, 0,\, 0)$ m, for $r = 1, \ldots, 30$, up to a total simulation time $T = 120$ s at a sampling rate of 0.01 s. This means that the Ricker pulse propagates through the domain Ω four times along the *x*-direction. Note that in principle we solve a 1-D wave propagation problem, however, we compute it in a fully 3-D elastic volume discretized by different unstructured tetrahedral meshes. In each mesh, the orientations of the single elements and their interfaces are different and never aligned to one of the coordinate axes, which represents the same case as in a real application as unstructured meshes can never be aligned to any space direction.

The analytical solution for the test cases is obtained by simply shifting the given Ricker wavelet in time with respect to the corresponding receiver position and its theoretical arrival time, which are known exactly. Note that the synthetic seismograms contain the propagating Ricker pulse periodically every 30 s due to the periodicity of the domain Ω. Therefore, we cut out seismogram intervals of 2000 time samples, that is, 20 s centred around the theoretical arrival time of the peak amplitude to analyse the misfits. This ensures that the seismograms well include the wavelet and numerical dispersion effects but avoids contaminating effects due to the periodicity of the signal. An example seismogram computed using Mesh 6 with an ADER-DG $\mathcal{O}5$ scheme is shown in Fig. 3(a) for receiver 1, where the Ricker pulse passes four times while continuously

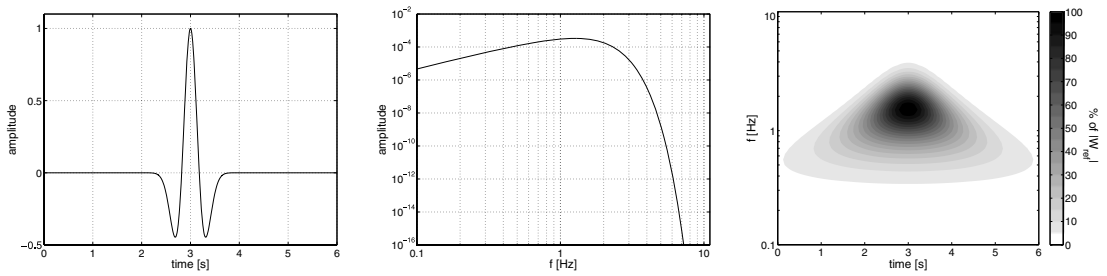

(a) (b) (c)

Figure 2. (a) Ricker-type pulse in the time domain, used for the accuracy study in the elongated computational domain Ω. (b) Fourier spectrum of the Ricker pulse. (c) The time–frequency representation of the Ricker signal obtained as the absolute value of the continuous wavelet transform.

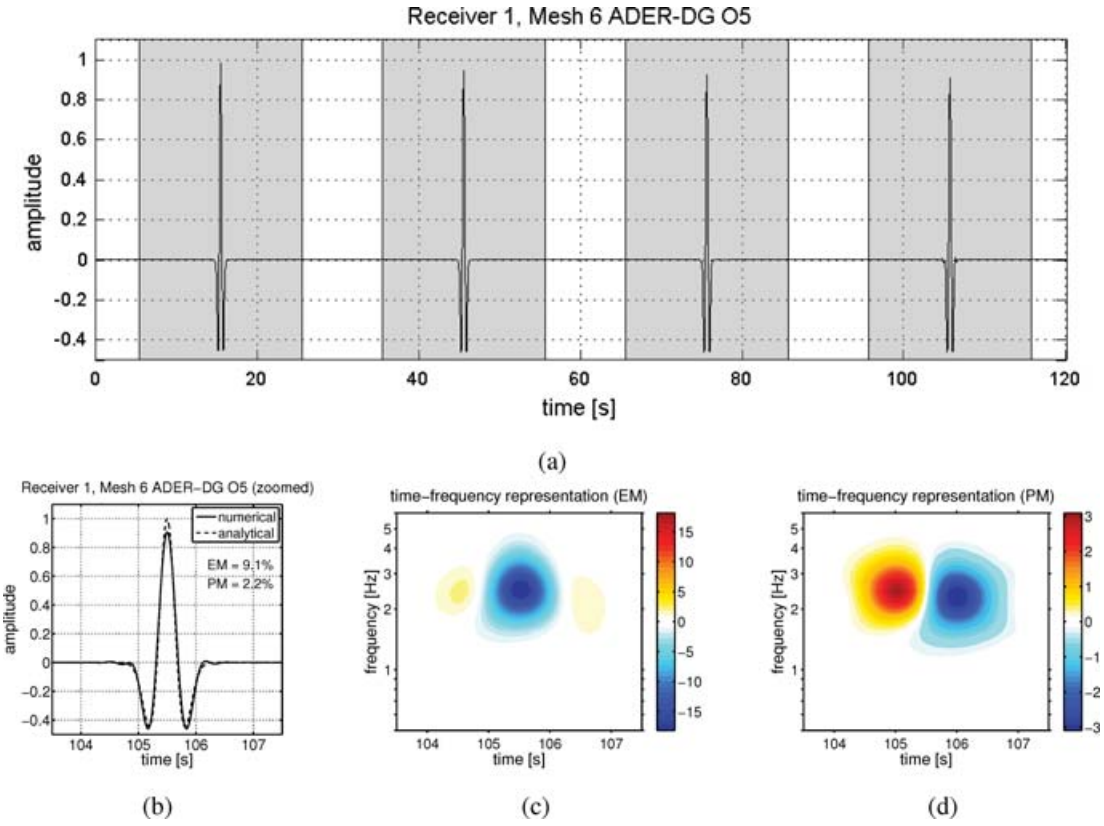

Figure 3. (a) Seismogram computed using Mesh 6 with an ADER-DG $\mathcal{O}5$ scheme at receiver 1 at $(-14.5, 0, 0)$ m where the maximum of the Ricker pulse passes for the first time at 15.5 s and then periodically in intervals of 30 s. Note the decrease in the maximum amplitude and the increase of numerical dispersion effects. The analysis intervals of the lengths of 20 s are shown as grey shaded regions. (b) A zoomed view of the numerical solution (solid) in (a) at the last passage of the Ricker pulse at receiver 1 at 105.5 s in comparison with the analytical solution (dashed), together with the EM and PM values. (c) Colour-coded time–frequency representation in of the EM given in per cent from 0.5 to 6 Hz and in the same time interval as (b). (d) Colour-coded time–frequency representation of the according PM.

losing amplitude and producing slightly more dispersion errors. An enlarged comparison to the analytical solution after the fourth passage is shown in Fig. 3(b). This plot also shows the single-valued EM and PM values for this comparison and confirms that the size of the analysis interval of 20 s for each pulse is large enough to avoid the influence of the periodic signal. We remark that this also holds true for seismograms computed with ADER-DG $\mathcal{O}2$ schemes on the coarsest Mesh 2. Figs 3(c) and (d) show the TFR of the EM and PM, respectively, in a frequency range from 0.5 to 6 Hz and in the same time interval 103.5–107.5 s as chosen for Fig. 3(b). We observe that the amplitude error attributed to the EM is about four times larger than the phase error given by the PM. In particular, Fig. 3(c) nicely shows a strong minimum in blue around the theoretical arrival time 105.5 s of the peak amplitude. There most of the amplitude is lost, while towards both sides of this minimum, light red maxima highlight the spurious oscillations. Fig. 3(d) instead shows a positive and a negative local extremum indicating that the first numerical phase arrives slightly too fast and then disappears too late, after the peak of the pulse has passed. However, at the peak passage time at 105.5 s, the TFR of the PM is almost zero throughout the whole frequency band. These plots also help to get a 'feeling' about the size of the EM and PM values obtained by integrating over the time and frequency axes, and their relation to the visual seismogram difference. For a presentation of a systematic study of the TFR of amplitude- and phase-modified simple wavelets, we refer to the work of Kristeková *et al.* (2006).

3 RESULTS

We present the accuracy results for the different simulations to show the dependence on approximation order, mesh spacing and propagation distance. To this end, we first consider the EM between the numerical and analytical seismograms as given in eq. (3).

In Fig. 4, we plot the results obtained on nine of the eleven different meshes indicated by k leading to a spatial sampling of $N_k \in [0.8, 1.2, 1.6, 2.0, 2.4, 3.2, 4.0, 4.8, 7.2]$, respectively. Each plot shows how the EM increases with the propagation distance. The symbols indicate the EM at the receiver positions and the different symbol types denote the different orders of approximation of the used ADER-DG scheme as given in the legend. Furthermore, we observe that some of the lines contain data points that deviate from the general trend. Analysing our results with respect to such outliers shows that they correlate to very particular or even extreme positions of a receiver within a tetrahedral element. This means that for a receiver position very close to the element edge or, especially, to an element vertex, that is, in the corner of a tetrahedral element, the accuracy might be decreased due to the behaviour of the approximation polynomial. We remark that in contrast to many other nodal-based numerical schemes (e.g. SEM) with nodes at the element edges and corners, the DG approach uses a modal basis, which is not connected to particular integration points inside an element. Therefore, it is difficult to control or predict the behaviour of very high-order polynomials at such special positions. Furthermore, we remark that due to the

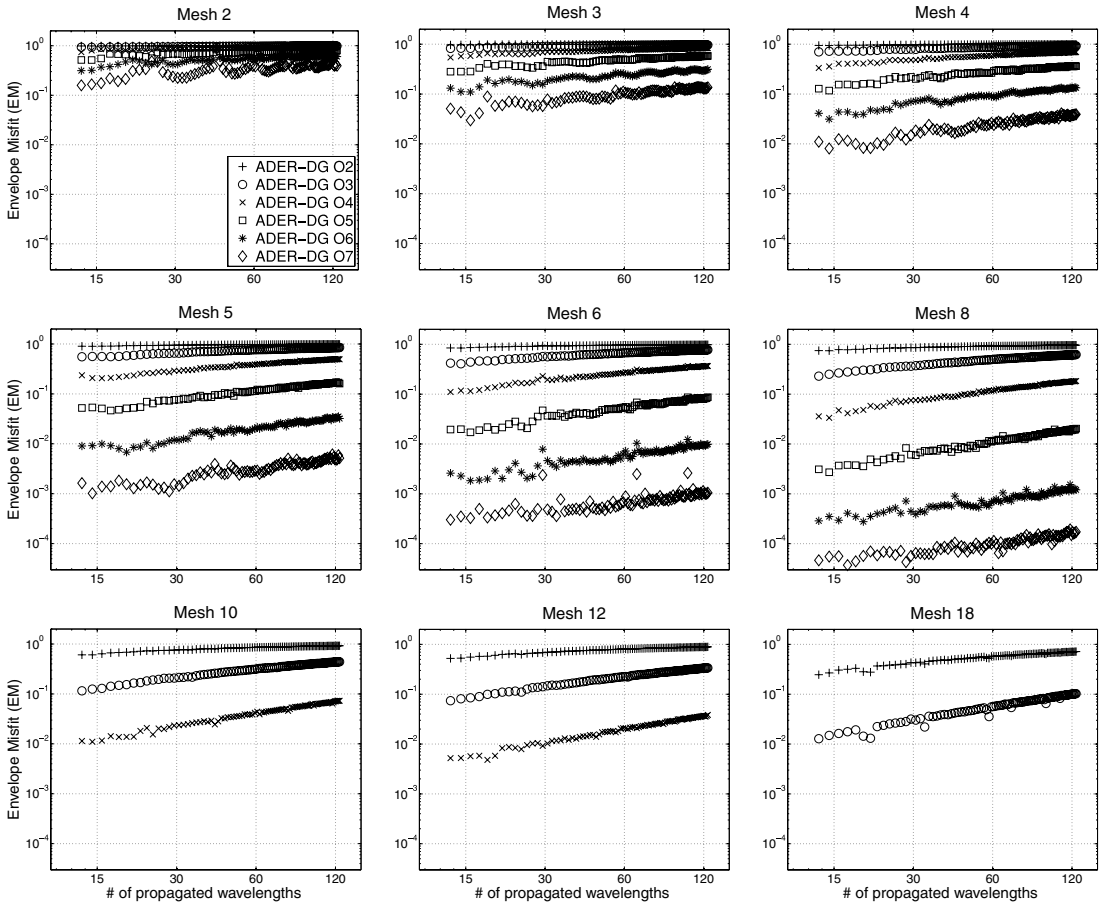

Figure 4. Envelope misfit depending on the propagation distance, given as the number of propagated dominant wavelengths λ_d and different orders of accuracy. Each of the different meshes indicated by k provides a spatial sampling of $N_k = 0.4\,k$ elements per dominant wavelength.

logarithmic scale of the EM in Fig. 4, the variation of the misfits for higher approximation orders are visually enhanced. We observe that the accuracy might sometimes also be slightly higher at some positions compared with the surrounding data points, especially visible in the results for the highest-order schemes using Mesh 8 and Mesh 18. These effects seem to depend on an incidental combination of the degree of the approximation polynomial and the receiver location. They do not appear systematically on the same mesh and the same receiver for all orders. Nevertheless, this location effect always remains relatively small and the error variation due to different locations is much less than the error difference between two subsequent orders (see Fig. 4).

Let us define the limit of an acceptable EM, represented in the plots of Fig. 4 as the constant line at EM $=10^{-2} = 1$ per cent. This is of course an arbitrary choice for our synthetic study here. In practical applications the acceptable accuracy limit should always be one order of magnitude below the accuracy of the modelling parameters (e.g. velocity structure, attenuation properties, etc.) as suggested by Ampuero & Nissen-Meyer (2008), to make sure that the numerical error does not dominate. We observe that Mesh 2 and 3 are definitely too coarse to obtain reasonably accurate results, even with the ADER-DG $\mathcal{O}7$ scheme. For Mesh 4 the ADER-DG $\mathcal{O}7$ scheme reaches the desired accuracy just for propagation distances of less than 20 wavelengths. On finer meshes, the misfits gradually decrease for each scheme as expected; however, for the lower-order ADER-DG $\mathcal{O}2$ and ADER-DG $\mathcal{O}3$ schemes, even the finest Mesh 18 is still too coarse to reach EM $= 1$ per cent. Due to the high accuracy of the higher-order schemes, we show only the results for the orders below $\mathcal{O}5$ for Mesh 10 and 12 and only results for orders below $\mathcal{O}4$ for the finest Mesh 18 to keep the same scaling of the y-axes. However, this trend continues to machine precision as shown in previous work (Dumbser & Käser 2006; Käser & Dumbser 2006). A further observation is that for a chosen mesh and approximation order, the misfits increase continuously but rather slowly with longer propagation distances. On the other hand, over the range of propagation distances investigated in this study, the misfits of two schemes of subsequent approximation orders can differ by one order of magnitude and this difference remains quite stable.

Considering the PM as given in eq. (3), we obtain similar results shown in Fig. 5. However, when comparing the plots of the EM and PM, we see systematically smaller values for the PM, which means that the numerical dispersion is less than numerical dissipation obtained by ADER-DG schemes and confirms the result shown explicitly in Fig. 3(b). This fact allows us to conclude that, if correct amplitudes are less important than phases, coarser meshes could be used. Nevertheless, the previous statements made for the EM in Fig. 4 do also apply for the PM in Fig. 5.

Now, let us look at our results from a different perspective. In Fig. 6 we plot, as typical for convergence tests, the EM and PM versus the number N_k of elements per wavelength for different orders of accuracy and for different propagation distances. The symbols again indicate the approximation order as before, whereas the different

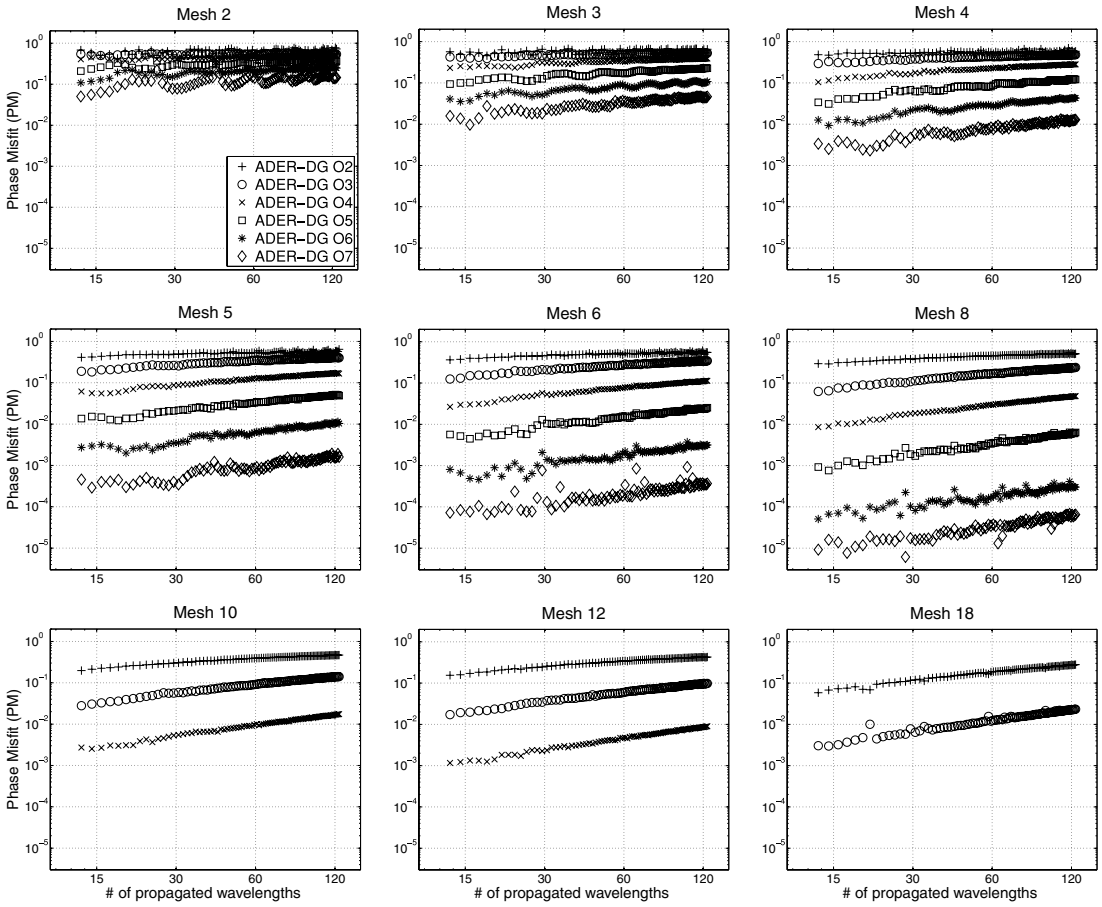

Figure 5. Phase misfit depending on the propagation distance, given as the number of propagated dominant wavelengths λ_d, and different orders of accuracy. Each of the different meshes indicated by k provides a spatial sampling of $N_k = 0.4\,k$ elements per dominant wavelength.

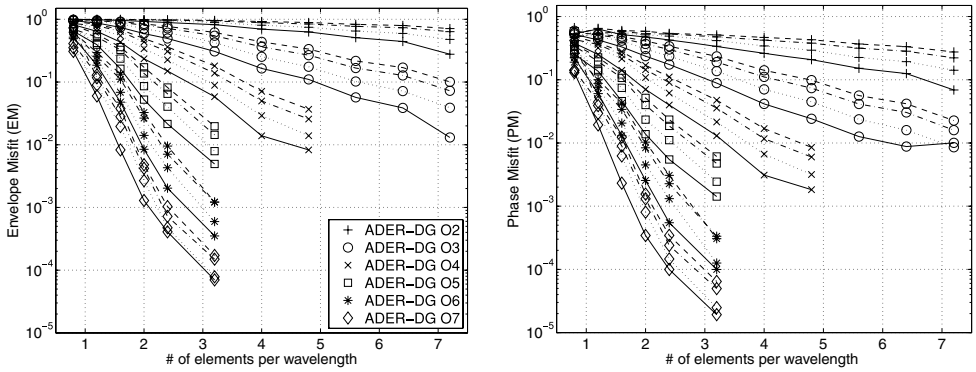

Figure 6. Envelope (a) and phase (b) misfits depending on the spatial sampling for different orders of accuracy and varying propagation distances, that is, for 20 (solid), 40 (dotted), 80 (dash-dotted) and 120 (dashed) propagated wavelengths.

line styles represent different propagation distances of 20 (solid), 40 (dotted), 80 (dash-dotted) and 120 (dashed) dominant wavelengths λ_d. Both plots in Figs 6(a) and (b) clearly show the faster decrease of misfits for the higher-order methods with the increasing spatial sampling rate N_k, that is, for decreasing mesh spacing h. For the ADER-DG $\mathcal{O}2$ and ADER-DG $\mathcal{O}3$ schemes, there is little improvement from 0.8 to 7.2 elements per wavelength and a much higher spatial sampling rate would be necessary to reach the desired misfit level of EM = 1 per cent. In general, we show that especially for lower-order schemes, the number of elements per wavelength for a scheme of order n always has to be increased considerably to reach the accuracy of a scheme of order $n + 1$. Furthermore, we now observe more clearly that the misfit obtained by a scheme of order n for only 20 propagated wavelengths is larger than the misfit obtained by a scheme of order $n + 1$ even for 120 propagated wavelengths. Note that this statement is valid for both EM and PM,

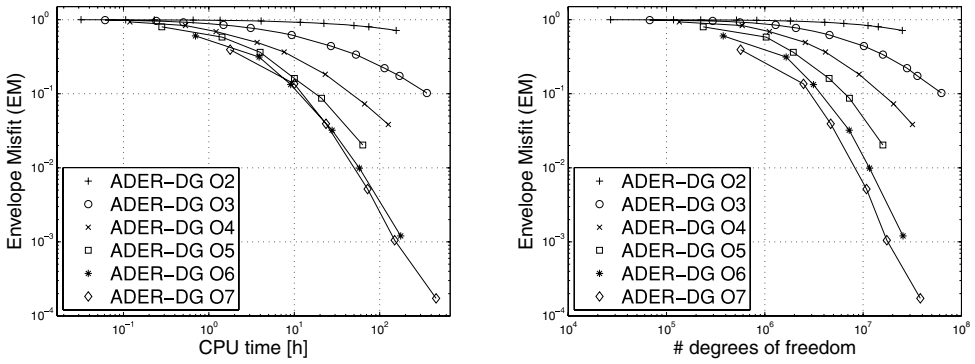

Figure 7. Envelope misfit (a) depending on the required CPU time to reach the final simulation time of $T = 120$ for a parallel computation on 8 Intel Itanium2 Montecito Dual Core 1.6 GHz cores and (b) depending on the required total number of degrees of freedom, which is proportional to the memory required.

whereas the values of the PM are systematically smaller than those of the EM. This means that higher-order schemes should always be preferred even when propagating only short distances, as the propagation distance obviously has a smaller influence on the accuracy than the chosen order.

However, even if these results strongly recommend the use of the higher-order ADER-DG schemes regarding the high accuracy of results, the most important issue is to analyse the schemes also with respect to their computational cost. The cost per element clearly increases for higher orders of approximation and the time step length decreases according to the stability criterion

$$\Delta t < \frac{1}{2d+1} \cdot \min_e \frac{2r_e}{c_e}, \tag{4}$$

where r_e is the radius of the insphere of a tetrahedral element indexed by e, c_e is the maximum wave velocity arising in this element and d is the degree of the approximation polynomial. However, as observed before, with higher-order schemes, we can use coarser meshes and therefore reduce the total number of elements. The question therefore is whether the reduction in the number of elements can compensate for the increase in cost per element and the more restrictive time step criterion (eq. 4). We show in Fig. 7(a) the obtained EM versus the required CPU time to reach the final simulation time $T = 120$ for a parallel computation on 8 Intel Itanium2 Montecito 1.6 GHz cores. We remark, that only the ADER-DG $\mathcal{O}2$ and ADER-DG $\mathcal{O}3$ schemes have been applied to all eleven meshes, whereas the scheme ADER-DG $\mathcal{O}4$ was applied only on the first eight meshes and the high-order schemes ADER-DG $\mathcal{O}5$ to ADER-DG $\mathcal{O}7$ to the first six meshes. This explains the different numbers of data points of the graphs in Figs 7(a) and (b). Recalling our desired accuracy limit EM = 1 per cent, the plot shows that this accuracy is achieved with the ADER-DG $\mathcal{O}7$ scheme in the least computational time of about 50 h. In general, Fig. 7(a) gives a clear answer to the question posed above, as it demonstrates that the use of a scheme of order n usually requires less CPU time to reach a desired accuracy than a scheme of order $n - 1$. Therefore, the increased cost per element and the more restrictive time step criterion can even be overcompensated by the use of a coarser mesh consisting of less and larger elements. Fig. 7(b) shows the obtained EM versus the total number of degrees of freedom, which are a measure of the memory used during the computations. Memory requirements are typically very low for our implementation of the ADER-DG scheme and therefore are not considered in detail in this study. However, the number of degrees of freedom per element and variable is $(d + 1)(d + 2)(d + 3)/6$, where d is again the degree of the approximation polynomial. For details we refer to previous work (Dumbser & Käser 2006). Nevertheless, we see, also concerning the memory requirements, that it seems to be beneficial to use very high-order schemes, as the enormous reduction in mesh elements in 3-D overcompensates the additional memory needed by each single element.

In the following, we use the results of the accuracy study to check if they can be used reliably for more complex modelling setups, where heterogeneous material, *P* and *S* waves and free surface waves are present. Note that, of course, the results of the previous accuracy analyses have to be applied considering the shortest wave length expected.

4 APPLICATION TO SPICE CODE VALIDATION PROBLEMS

To validate our results of the accuracy analysis, we use the obtained information in the application of the ADER-DG schemes to two SPICE Code Validation problems, LOH.1 and LOH.3. To this end, we chose a desired seismogram accuracy that should be obtained by the simulation and discretize the model using a tetrahedral mesh spacing according to the expected wavelengths, the propagation distance and the selected approximation order.

4.1 LOH.1

For the LOH.1 test case, the surface layer and the half-space have minimum *S*-wave velocities of 2000 and 3464 m s^{-1}, respectively. As the source signal does not have a dominant frequency we use the maximum frequency of the signal, which is defined to be 5 Hz. The propagation distance from the double-couple point source to the considered receiver is about 10 km, that is, 5 km in the half-space and 5 km in the surface layer. Therefore, the total propagation distance is about 20 wavelengths for the wave with the shortest wavelength. We set the required accuracy to EM $\leq$ 10 per cent, which automatically should provide a smaller PM.

Then we can extract from Fig. 6 that we need 2.76, 1.78 or 1.39 elements per shortest wavelength for the estimated propagation distance when using an ADER-DG $\mathcal{O}4$, $\mathcal{O}5$ or $\mathcal{O}6$ scheme, respectively. Therefore, we generate three different tetrahedral meshes for three computations with the different approximation orders. The tetrahedra used by the ADER-DG $\mathcal{O}4$ scheme have an average edge length of 145 m in the layer and 251 m in the half-space according to

Table 1. Misfits of the radial (EM_r, PM_r), transversal (EM_t, PM_t) and vertical (EM_v, PM_v) velocity components for the LOH.1 and LOH.3 test cases.

	LOH.1			LOH.3		
	$\mathcal{O}4$	$\mathcal{O}5$	$\mathcal{O}6$	$\mathcal{O}4$	$\mathcal{O}5$	$\mathcal{O}6$
EM_r(%)	5.8	4.7	6.2	7.0	6.5	7.4
PM_r(%)	1.7	1.4	1.7	2.8	2.9	2.8
EM_t(%)	6.3	5.0	5.9	5.1	5.2	5.1
PM_t(%)	1.2	1.3	1.0	1.2	1.1	1.5
EM_v(%)	3.0	3.0	3.7	4.9	4.6	5.2
PM_v(%)	1.4	1.1	1.4	2.7	2.7	2.6

our analysis. The mesh respective spacings for the ADER-DG $\mathcal{O}5$ scheme are 225 and 389 m and for the ADER-DG $\mathcal{O}6$ scheme 288 and 498 m. The EM and PM of the obtained velocity seismograms with respect to the analytic frequency–wavenumber (FK) solutions (Day *et al.* 2003) for the radial, transversal and vertical components are given in Table 1. As expected, the values of the PM are always smaller than those of the EM. Furthermore, all misfits are clearly below the required 10 per cent, which is due to the consideration of the maximum frequency of 5 Hz in the setup. The dominant frequency of the signal, however, is lower and, therefore, explains the better results. The important fact is that the three computations of different orders give basically the same accuracy, which confirms that our accuracy analysis and the accordingly chosen mesh spacings are correct.

In Fig. 8, we show the TFR of the EM and PM (TFEM, TFPM) for the three components obtained with the ADER-DG $\mathcal{O}5$ scheme together with the comparison of the numerical and analytical seismogram in the time domain. The TFR of the misfits are shown in analogy to figs 7 and 8 of the work of Kristeková *et al.* (2006), who also provide the detailed description of the additionally used error norms: frequency-dependent EM and PM (FEM, FPM) and time-dependent EM and PM (TEM, TPM). Note, however, that the range of our colour scale and our misfit axes only span ± 10 per cent compared with $\pm$ 40 per cent used by Kristeková *et al.* (2006). Even though this comparison shows that our results are more accurate, one has to consider that these reference solutions (Kristeková *et al.* 2006) might not be the present-day results. Furthermore, there are no CPU-time comparisons available.

It is obvious that the largest misfits occur towards the end of our numerical seismogram at high frequencies, whereas the EM is much larger than the PM. Other investigations (Käser *et al.* 2007b) showed that this is due to the non-perfect absorbing boundary conditions that introduce spurious reflections after around 6 s and, therefore, significantly contributes to the EM and PM values.

4.2 LOH.3

In a further example, we apply the same three ADER-DG schemes with their corresponding meshes to the LOH.3 test case, which includes viscoelastic attenuation in the two materials. This allows us to compare our results directly with those presented by Kristeková *et al.* (2006). The analytical solutions are again provided by the FK method (Apsel & Luco 1983). The misfit values are given in Table 1. Compared with the LOH.1 case, the errors are slightly larger for the radial and vertical components but remain similar for the transversal component. However, even for viscoelastic wave propagation, our parameter setup with respect to the required accuracy is still valid. The TFR of the misfits obtained by the ADER-DG $\mathcal{O}5$ scheme for the three velocity components are shown in Fig. 9 in analogy to figs 7 and 8 of (Kristeková *et al.* 2006). Again, the range

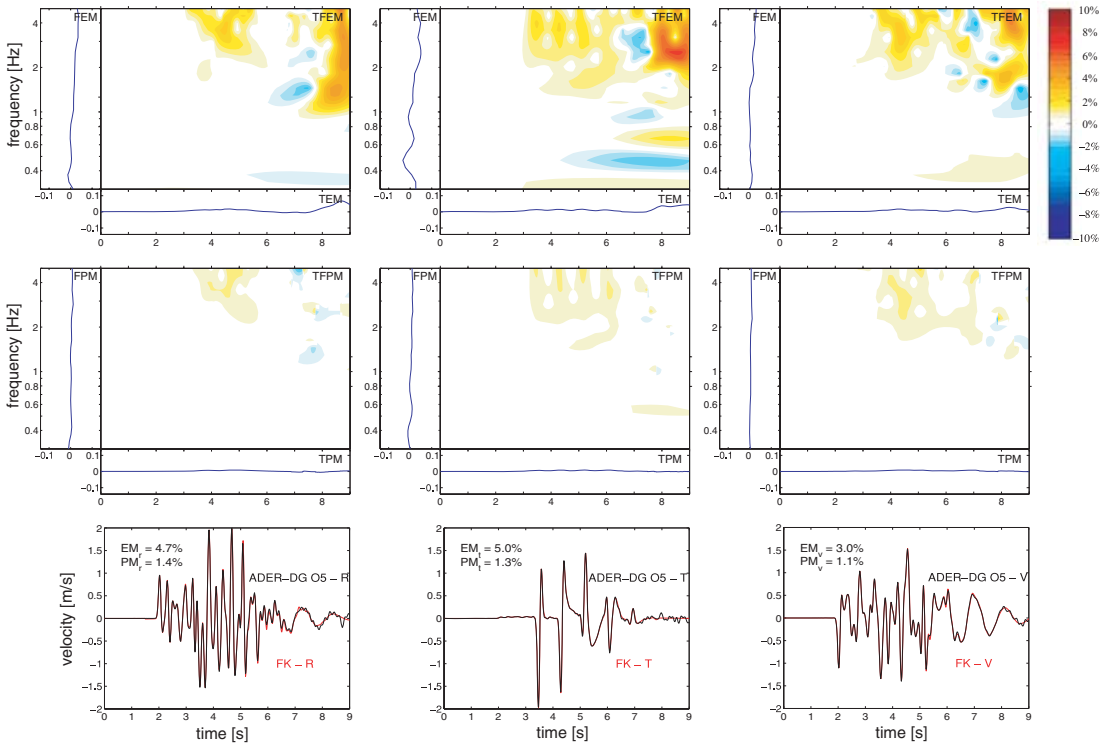

Figure 8. Time–frequency representation of the misfits of the radial (left), transversal (middle) and vertical (right) components of the velocity seismograms for the LOH.1 case. The comparison of the numerical (ADER-DG $\mathcal{O}5$, black) and the analytical (FK, red) seismograms is shown at the bottom, together with their single-valued EM and PM.

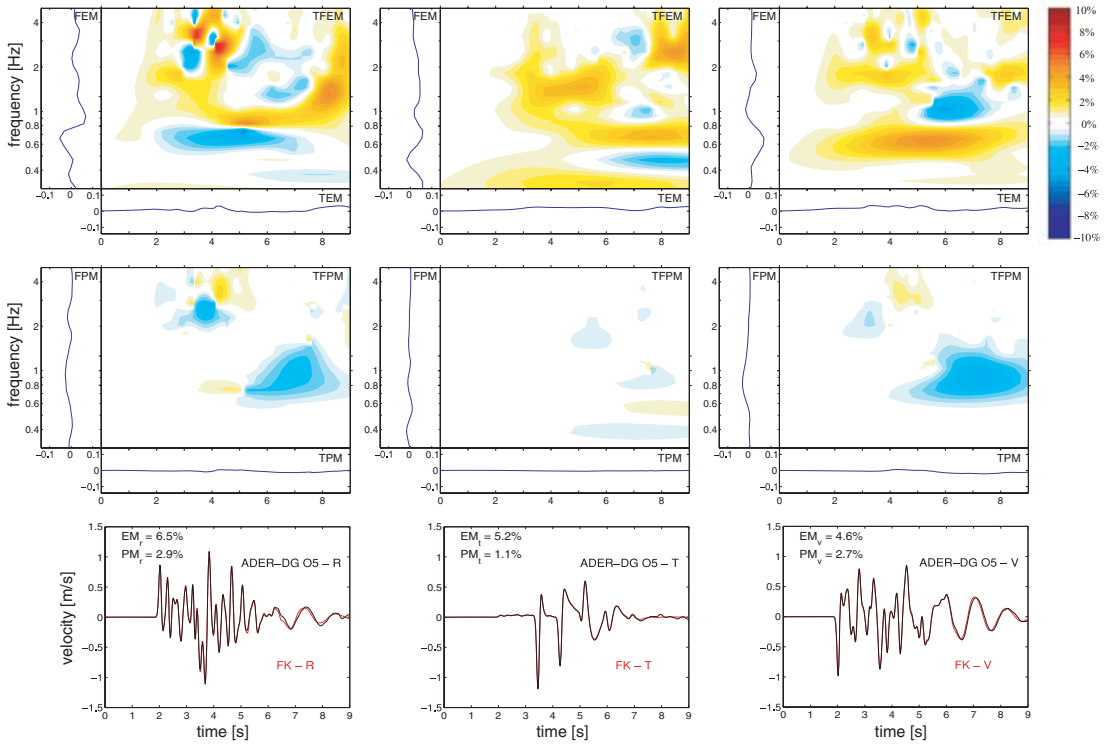

Figure 9. Time–frequency representation of the misfits of the radial (left), transversal (middle) and vertical (right) components of the velocity seismograms for the LOH.3 case. The comparison of the numerical (ADER-DG $\mathcal{O}5$, black) and the analytical (FK, red) seismograms is shown at them, bottom together with their single-valued EM and PM.

of our colour scale and our misfit axes only spans ± 10 per cent. Furthermore, the ADER-DG scheme shows clearly lower misfits in the high frequency band above 3 Hz than the methods compared by Kristeková *et al.* (2006). In particular, the PM values in Fig. 9 are very low compared with the EM and can hardly be seen at this scale for the transversal component. The actual seismic traces at the bottom of Fig. 9 show visual differences mainly towards the end after about 6 s. However, the TFR, especially of the EM, discovers amplitude problems basically throughout the whole duration of the seismogram also in the low frequency range. This seems to be similar, however much weaker in comparison with the results obtained by WCC1 and CMUN presented by Kristeková *et al.* (2006).

5 DISCUSSION

We presented a quantitative accuracy analysis for the ADER-DG scheme for the simulation of seismic wave propagation. We evaluated the interaction of the approximation order of the numerical scheme, the mesh spacing of the used discretization and the propagation distance of the waves, based on the time–frequency representation of the seismogram misfits. The results are obtained by a systematic variation of the different parameters on a simplified but 3-D test model. The outcome of the analysis, mainly summarized in Fig. 6, serves as a guideline for choosing the correct modelling parameters with respect to a required accuracy limit. Hereby, we found that for the ADER-DG method, the phase accuracy is always higher than the amplitude accuracy. Furthermore, we showed that in general, the use of the higher approximation orders in combination with coarser meshes is preferable as the reduction in the number of mesh elements dominates the increased cost per element and therefore reduces the total computation time. However, geometrical constraints such as a rough surface topography or internal structure might often prohibit the use of very coarse meshes and determine a certain mesh spacing that has to be used. Therefore, our study gives a clear relationship between the used mesh spacing, the expected propagation distance, the desired amplitude and phase accuracy and the finally chosen approximation order. The practical use of our analysis study is validated through the application of our results to the well-acknowledged test cases LOH.1 and LOH.3 of the SPICE Code Validation project, including heterogeneous elastic material, free surface boundary conditions and also viscoelastic attenuation. Defining a desired accuracy limit and simulating the wave propagation for a specified distance but using different meshes led for both test cases to the same expected results as the required approximation scheme could be chosen correctly.

Finally, as has been mentioned above, there is a number of numerical methods available to seismologists to solve wave propagation problems. These methods have become increasingly sophisticated and their computational implementations and efficiencies differ considerably. Therefore, it is difficult for a single scientist or group to use them all to their full capacity. A collective effort, where developers and experts of the various methods provide solutions to some established test cases, could clarify the picture of how the different approaches perform and how they compare with each other. Therefore, we encourage scientists in the community of numerical seismology to participate in the interactive SPICE Code Validation exercises and make use of the new misfit criteria directly accessible at www.nuquake.eu/SPICECVal. A number of test cases, analytical and reference solutions, including those of the ADER-DG method, are already available. A user can upload his locally computed solutions and their accuracy is automatically assessed. Additionally, the results are stored so that others can access them online. This

way, the different contributions create a database, where a comprehensive overview of the capabilities of contemporary methods for seismic wave propagation is offered to the rest of the seismological community.

ACKNOWLEDGMENTS

The authors thank the DFG (Deutsche Forschungsgemeinschaft), as the work was supported through the Emmy Noether-Program (KA 2281/2-1). The comments of the two reviewers Peter Moczo and Tarje Nissen-Meyer and the resulting fruitful discussions are appreciated and have helped to improve the manuscript. The support by the local system administrator J. Oeser when using the Linux-Cluster of our department is also appreciated. Furthermore, we thank the Leibniz-Rechenzentrum, where the LOH.1 and LOH.3 test cases have been computed.

REFERENCES

Ampuero, J.-P. & Nissen-Meyer, T., 2008. High order conservative time schemes in spectral element methods for seismic wave propagation, *submitted*.

Apsel, R. & Luco, J., 1983. On the Green's functions for a layered half-space, part II, *Bull. seism. Soc. Am.,* **73,** 931–951.

Bielak, J., Loukakis, K., Hisada, Y. & Yoshimura, C., 2003. Domain reduction method for three-dimensional earthquake modeling in localized regions. part I: Theory, *Bull. seism. Soc. Am.,* **93,** 817–824.

Bouchon, M. & Sánchez-Sesma, F.J., 2007. Boundary integral equations and boundary elements methods in elastodynamics, in *Advances in Wave Propagation in Heterogeneous Earth,* Vol. 48: Advances in Geophysics Series, pp. 157–189, eds Wu, R.-S. & Maupin, V., Elsevier, Academic Press, London, UK.

Carcione, J.M., 1994. The wave equation in generalised coordinates, *Geophysics,* **59,** 1911–1919.

Chaljub, E., Capdeville, Y. & Vilotte, J.-P., 2003. Solving elastodynamics in a fluid-solid heterogeneous sphere: a parallel spectral element approximation on non-conforming grids, *J. comput. Phys.,* **187**(2), 457–491.

Chaljub, E., Komatitsch, D., Vilotte, J.-P., Capdeville, Y., Valette, B. & Festa, G., 2007. Spectral-element analysis in seismology, in *Advances in Wave Propagation in Heterogeneous Earth,* Vol. 48: Advances in Geophysics Series, pp. 365–419, eds Wu, R.-S., Maupin, V. & Dmowska, R. (series ed.), Elsevier, Academic Press, London, UK.

Day, S., Bielak, J., Dreger, D., Graves, R., Larsen, S., Olsen, K. & Pitarka, A., 2003. *Tests of 3-D elastodynamic codes,* Final report for Lifelines Project 1A02, Tech. Rep., Pacific Earthquake Engineering Research Center.

de la Puente, J., Käser, M., Dumbser, M. & Igel, H., 2007. An arbitrary high order discontinuous Galerkin method for elastic waves on unstructured meshes – IV: Anisotropy, *Geophys. J. Int.,* **169**(3), 1210–1228.

Dumbser, M. & Käser, M., 2006. An arbitrary high order discontinuous Galerkin method for elastic waves on unstructured meshes II: the three-dimensional case, *Geophys. J. Int.,* **167**(1), 319–336.

Dumbser, M., Käser, M. & Toro, E.F., 2007. An arbitrary high order discontinuous Galerkin method for elastic waves on unstructured meshes V: p adaptivity and local time stepping, *Geophys. J. Int.,* **171**(2), 695–717.

Fornberg, B., 1975. On a fourier method for the integration of hyperbolic equations, *SIAM, J. Numer. Anal.,* **12,** 509–528.

Fornberg, B., 1987. The pseudospectral method: comparisons with finite differences for the elastic wave equation, *Geophysics,* **52**(4), 483–501.

Fornberg, B., 1996. *A Practical Guide to Pseudospectral Methods,* Cambridge University Press, Cambridge.

Gallovič, F., Barsch, R., de la Puente Alvarez, J. & Igel, H., 2007. Digital library for computational seismology, *EOS,* **88**(50), 559.

Geller, R.J. & Takeuchi, N., 1995. A new method for computing highly accurate DSM synthetic seismograms, *Geophys. J. Int.,* **123,** 449–470.

Geller, R.J. & Takeuchi, N., 1998. Optimally accurate second-order time-domain finite difference scheme for the elastic equation of motion: one-dimensional case, *Geophys. J. Int.,* **135,** 48–62.

Holschneider, M., 1995. *Wavelets: An Analysis Tool,* Oxford Science Publications, Oxford.

Käser, M. & Dumbser, M., 2006. An arbitrary high order discontinuous Galerkin method for elastic waves on unstructured meshes I: the two-dimensional isotropic case with external source terms, *Geophys. J. Int.,* **166**(2), 855–877.

Käser, M., Dumbser, M., de la Puente, J. & Igel, H., 2007a. An arbitrary high order discontinuous Galerkin method for elastic waves on unstructured meshes - III, viscoelastic attenuation, *Geophys. J. Int.,* **168**(1), 224–242.

Käser, M., Mai, P. & Dumbser, M., 2007b. On the accurate treatment of finite source rupture models using ADER-DG on tetrahedral meshes, *Bull. Seism. Soc. Am.,* **97**(5), 1570–1586.

Komatitsch, D. & Vilotte, J.P., 1998. The spectral-element method: an efficient tool to simulate the seismic response of 2-D and 3-D geological structures, *Bull. seism. Soc. Am.,* **88,** 368–392.

Komatitsch, D., Liu, Q., Tromp, J., Süss, P., Stidham, C. & Shaw, J.H., 2004. Simulations of ground motion in the Los Angeles basin based upon the spectral element method *Bull. seism. Soc. Am.,* **94**(1), 187–206.

Koketsu, K., Fujiwara, H. & Ikegami, Y., 2004. Finite-element simulation of seismic ground motion with a voxel mesh, *Pure appl. geophys.,* **161,** 2183–2198.

Kristek, J. & Moczo, P., 2006. On the accuracy of the finite-difference schemes: the 1d elastic problem, *Bull. seism. Soc. Am.,* **96**(6), 2398–2414.

Kristeková, M., Kristek, J., Moczo, P. & Day, S., 2006. Misfit criteria for quantitative comparison of seismograms, *Bull. seism. Soc. Am.,* **96**(5), 1836–1850.

Madariaga, R., 1976. Dynamics of an expanding circular fault, *Bull. seism. Soc. Am.,* **65,** 163–182.

Marfurt, K., 1984. Accuracy of finite-difference and finite-element modeling of the scalar and elastic wave equations, *Geophysics,* **49,** 533–549.

Moczo, P., Kristek, J., Vavrycuk, V., Archuleta, R.J. & Halada, L., 2002. 3-D heterogeneous staggered-grid finite-difference modeling of seismic motion with volume harmonic and arithmetic averaging of elastic moduli and densities, *Bull. seism. Soc. Am.,* **92**(8), 3042–3066.

Moczo, P., Kristek, J., Galis, M., Pazak, P. & Balazovjech, M., 2007a. The finite-difference and finite-element modeling of seismic wave propagation and earthquake motion, *Acta physica slovaca,* **57**(2), 177–406.

Moczo, P., Robertsson, J.O.A. & Eisner, L., 2007b. The finite-difference time-domain method for modeling of seismic wave propagation. In *Advances in Wave Propagation in Heterogeneous Earth,* Vol. 48: Advances in Geophysics Series, pp. 421–516, eds, Wu, R.-S. & Maupin, V., Dmowska, R. (series ed.), Elsevier, Academic Press, London, UK.

Saenger, E.H., Gold, N. & Shapiro, S.A., 2000. Modeling the propagation of elastic waves using a modified finite-difference grid, *Wave Motion,* **31,** 77–92.

Saenger, E.H. & Bohlen, T., 2004. Finite-difference modeling of viscoelastic and anisotropic wave propagation using the rotated staggered grid, *Geophysics,* **69,** 583–591.

Seriani, G. & Priolo, E., 1994. Spectral element method for acoustic wave simulation in heterogeneous media, *Finite Element Anal. Des.,* **16,** 337–348.

Virieux, J., 1984. SH wave propagation in heterogeneous media: velocity-stress finite-difference method, *Geophysics,* **49,** 1933–1942.

Virieux, J., 1986. P-SV wave propagation in heterogeneous media: velocity-stress finite-difference method, *Geophysics,* **51,** 889–901.

Yoshimura, Ch., Bielak, J., Hisada, Y. & Fernández, A., 2003. Domain reduction method for three-dimensional earthquake modeling in localized regions, Part II: Verification and applications, *Bull. seism. Soc. Am.,* **93**(2), 825–840.